Journal of Environmental Health Science and Engineering (2022) 20:861–879
https://doi.org/10.1007/s40201-022-00827-w

RESEARCH ARTICLE

Adsorption of arsenic in aqueous solution onto iron impregnated bagasse fly ash

Sundaramurthy Suresh[1] · Mika Sillanpää[2,3,4] · Fawzi Banat[5] · Ravi Kiran Vissa[6]

Received: 2 December 2020 / Accepted: 9 August 2022 / Published online: 23 August 2022

Abstract

The present study examined the adsorption of As(III) and As(V) (arsenics) from aqueous solutions using $FeCl_3$ impregnated bagasse fly ash (BFA-Fe). Batch adsorption studies were carried out to evaluate the effect of various parameters like initial pH (pH_0), adsorbent dose (m), contact time (t), initial concentration (C_0) and temperature (T) on the removal of As(III) and As(V) from aqueous solutions. The maximum removal of As(III) and As(V) was found ~ 95% and ~ 97% at lower concentration (< 20 µg/dm^3) and ~ 86% and ~ 87% at higher concentration (500 µg/dm^3), respectively, using 3 g/dm^3 of BFA dosage at 303 K. The adsorption of arsenics on BFA-Fe was very rapid. Pseudo-second-order kinetic model well represented the adsorption kinetics of both As(III) and As(V). Error analyses functions for adsorption of As(III) and As(V) onto BFA-Fe. Based on these error analyses, R-P isotherm was found to be fitted. Thermodynamic parameters, i.e., ΔG°, ΔH°, and ΔS°, were also calculated. At 25.0 to 45.0 °C, the values of ΔG° lie in the range of -43.85, -45.34, -48.82, -51.31, -53.8, and -44.75, -48.3, -51.84, -55.39, -58.93, -55.57 for As (III), and As (V) respectively, indicating that adsorption is spontaneous and exothermic in nature. Regeneration study was carried out by different solvent and thermal methods. Our results revealed that BFA-Fe can be reused directly for making fire-briquettes to explore its energy value. From this study, As containment is most effective removal from aqueous solution and mimic to any contaminated water resources.

Keywords Arsenic ions · Effect of temperature · Bagasse fly ash · Ferric chloride · Isotherms

Introduction

Water is the essential chemical substance in all living and non-living organisms for the survival of life. According to the UNICEF census report in the year of 2019, 2.2 billion people still lack access to healthy drinking water, and the percentage contribution of different parts of the world [1]. Due to geological natural processes and adverse anthropogenic activities, like industrialization, urbanization, improper management of waste, heavy metals, Arsenic (As) originating in the ground water [2–6]. In other side, tube wells accelerating As through diffusion process from the ground water, a way to entering in the food products such as wheat, barley, and rice and also increasing toxic stimulating via biological magnification [7].

As is basically in inorganic form in the ground water which denoted by arsenite and arsenate (As (III), As (V)) [8, 9]. The agencies has classified As as Class I human carcinogen pollution [10, 11]. These As are poisonous nature which has chronic exposure (permissible limit less than 0.05 mg/l)

✉ Sundaramurthy Suresh
ssureshchemengg@gmail.com; sureshs@manit.ac.in

✉ Mika Sillanpää
mikaetapiosillanpaa@duytan.edu.vn

1 Department of Chemical Engineering, Maulana Azad National Institute of Technology Bhopal, MP 462 003 Bhopal, India

2 Institute of Research and Development, Duy Tan University, Da Nang 550000, Vietnam

3 Faculty of Environment and Chemical Engineering, Duy Tan University, Da Nang 550000, Vietnam

4 Department of Chemical Engineering, School of Mining, Metallurgy and Chemical Engineering, University of Johannesburg, P. O. Box 17011, Doornfontein 2028, South Africa

5 Department of Chemical Engineering, Khalifa University of Science and Technology, Abu Dhabi, United Arab Emirates

6 Process Engineer, L&T AdVENT, Larsen & Toubro Ltd. Powai, Mumbai 400 072, India

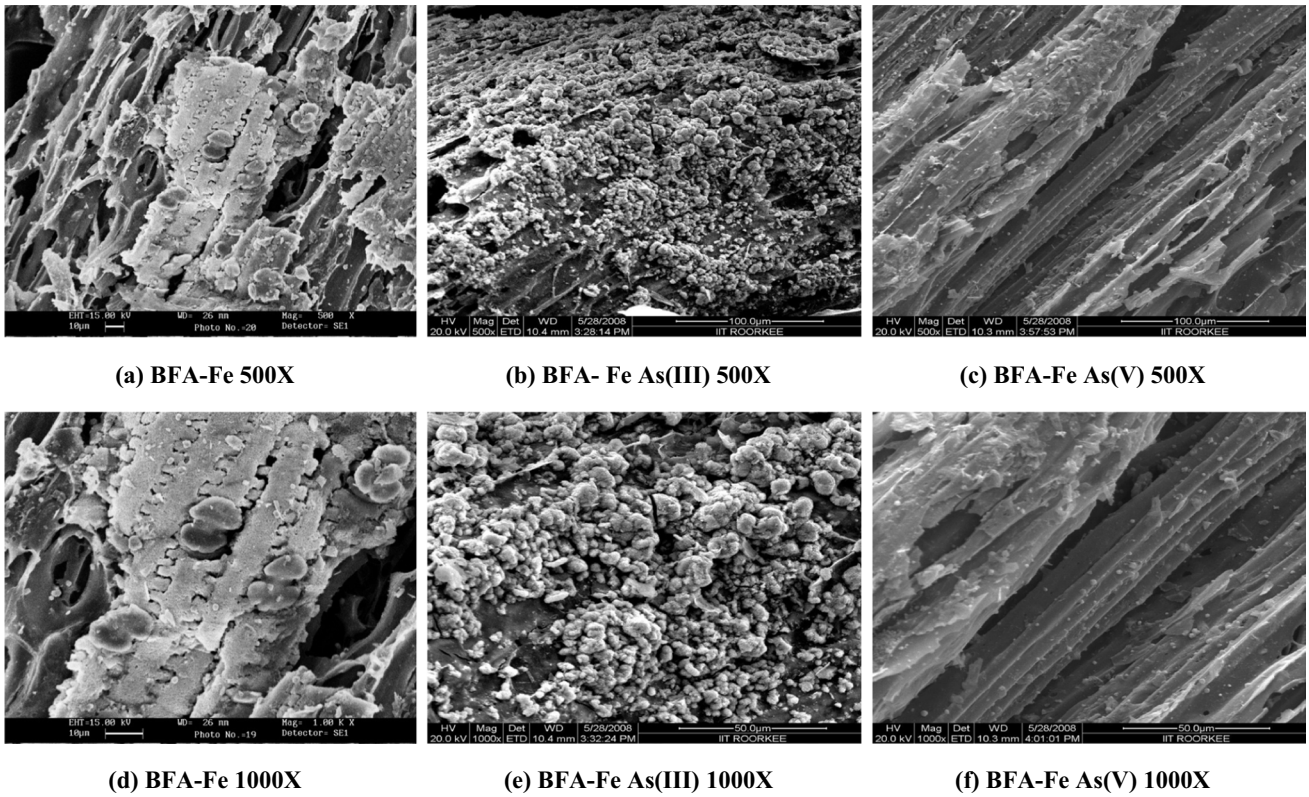

Fig. 1 SEM of blank, As(III) and As(V) loaded BFA-Fe at 500X and 1000X

leads different human diseases like cancer, neurological, and respiratory, etc. [3, 12–16].

It has been reported in the several countries which As contain at high levels in groundwater. Podgorski and Berg [15] reported India has more than twenty five water sites which risk of exposure of As toxicity. For example, study reported dominancy of As (III) in the ground water specially Bangladesh, Central India [17]. World health organisation and Indian standard [11, 18] recommends less than 10 µg/L of As concentration in the drinking water have less toxicity. Chakrabarti et al. [19] reported more than 200 million population has unfortunate to consumption of higher side of As containing drinking water.

Therefore, promising As removal technologies needs to overcome these factors through low-cost, reliable and sustainable ways. Some major arsenic removal technologies are chemical oxidation [20], flocculation [21], adsorption [22–26], biosorption [3–5, 27], photo-oxidation [28], and ion-exchange techniques [29], Membrane techniques [21, 30–36]. For example, Bahmani et al. [33] reported As removal through nano-filtration has higher efficiency. However, membrane process and ion exchange method are usually takes removal at higher cost. Moreover, fouling of membrane causes double the cost of operation. The secondary pollution generated from different chemical oxidation or reduction, and precipitation processes. In simple, handling and reliable cost, the adsorption treatment method for As removal from water stream makes best out of treatment choice.

Material science and engineering, now-a-days play a major role for developing novel adsorbent from different source or low-cost. Several adsorbents are used by researchers for removal of As(V) and As(III) water, such as activated carbon [37], biochar [38], Mango leaf and rice husk powder [3], palm bark biomass [4], Psidium guajava leaf surface [5], and zeolite [39]. Among all the adsorbents, industrial by-product like bagasse fly ash (BFA) from sugar mill, is one of the cheapest adsorbents reported to be efficient in removing organic compounds, dyes, phenols, heavy metals,

Table 1 Physical characteristics of adsorbent

Characteristics	BFA-Fe
Proximate analysis	
Moisture (%)	13.39
Volatile matter (%)	10.80
Ash (%)	55.22
Fixed Carbon (%)	19.59
Bulk density (kg m^{-3})	133.3
Average particle size (µm)	381.45

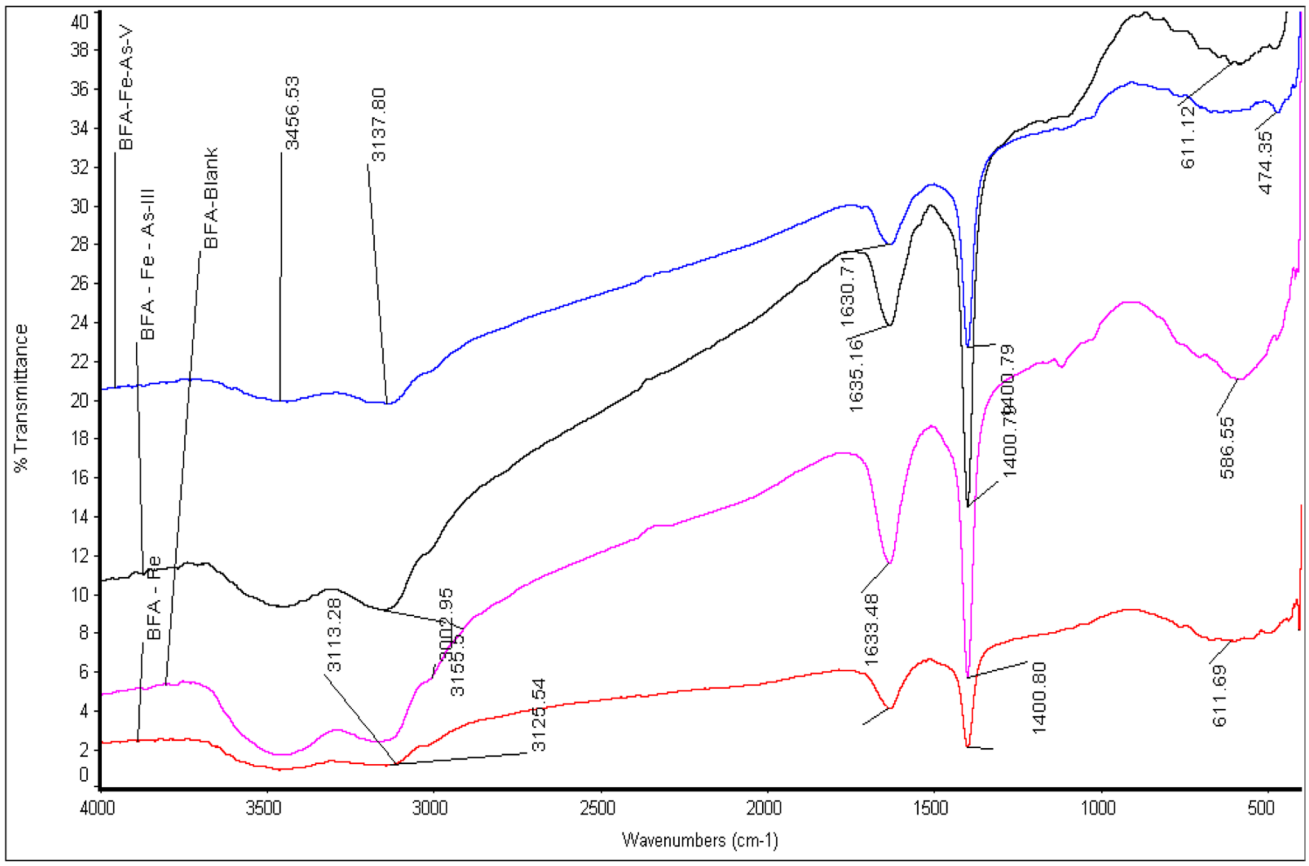

Fig. 2 FTIR spectra of blank, As(III) and As(V) loaded BFA-Fe

etc.[40, 41]. Adsorption of arsenic onto granular activated carbon surface was very low due to its negatively charged [42]. The chemicals like H_3PO_4, H_2SO_4, KOH, NaOH and $ZnCl_2$ of were used for activation or impregnation of absorbent for removing foreign impurities and improving surface properties [43].

The impregnated adsorbent especially iron based has promosing material for remvoal of As due its nature of good magnetic and affinity towards arsenic and high efficiency in reported [44]. Ocinski and Mazur [45] studied removal of As (V) through modified coal fly ash into Fe–Mn and composite with help of chitosan matrix and found good efficiency. Muniz et al. [46] reported iron impregnated activated carbon showed good adsorptive of As ions from the water. This is due to advantage of combine properties of high surface area of activated carbon with iron nanoparticles. Kleinert et al. [47] reported the difference in the removal efficiency of As (V) through biogenic and abiogenic iron oxy-hydroxide surfaces and found abiogenic iron based adsorbent is more efficient than any other one.

Table 2 Elemental composition of adsorbent before and after adsorption

Element	Weight %		
	BFA-Fe	BFA-Fe-As(III)	BFA-Fe-As(V)
C	37.99	24.49	24.70
O	17.32	18.5	19.23
Si	2.00	0.34	0.00
Cl	10.44	14.79	16.61
Fe	32.25	40.48	39.17
As	0.00	1.40	0.30

No literature available on the adsorptive removal of arsenite and arsenate by using iron impregnated BFA as an adsorbent. Based on this adsorption factors, study was carried out for As(III)) and As (V) adsorption onto Fe-BFA. Arsenic adsorption through different process affecting parameters such as pH, mass of the dosage, time, arsenic concentration, and temperature have been investigated. Equilibrium isotherms have been tested with different isotherm equations and chemical thermodynamics data was generated. To test model equations adequacy and accuracy on experimental datas, different error analysis has also been carried out. Finally, chemical and thermal regeneration studies was performed for understanding recyclability of spent Fe-BFA.

Materials and methods

Adsorbent and its characterization

The BFA, obtained from Northern part of sugar mills (India) which was washed with hot water (70 ºC), dried, soaked in 1 M $FeCl_3$ solution for 24 h, then dried again (BFA-Fe) and used for As(III) and As(V) removal in a batch mode. The BFA-Fe characteristics were determined using standard procedure (IS: 1350–1984, part-I). To determine surface morphology of samples, scanning electron microscope (SEM, LEO 435 VP) used.

To determine the functional groups, Fourier Transform Infrared (FTIR) spectrophotometer was used (Thermo micolet Model Magna 760) using pellet (pressed disk) technique. The pellets were prepared with KBr. The spectral range covered was from 4000 to 400 cm^{-1}. The thermal degradation characteristics of BFA-Fe and spent BFA-Fe (after adsorption) has been determined by a Perkin Elmer TGA analyzer. The mass loss of the solid sample was continuously monitored as the sample followed a linear heat up programme (100 K/min) at 200 ml/min gas flow rate. The sample (about 5 mg) was uniformly spread over the crucible base. The BET surface area of BFA-Fe was estimated by the standard adsorption of N_2 at 77.15 K.

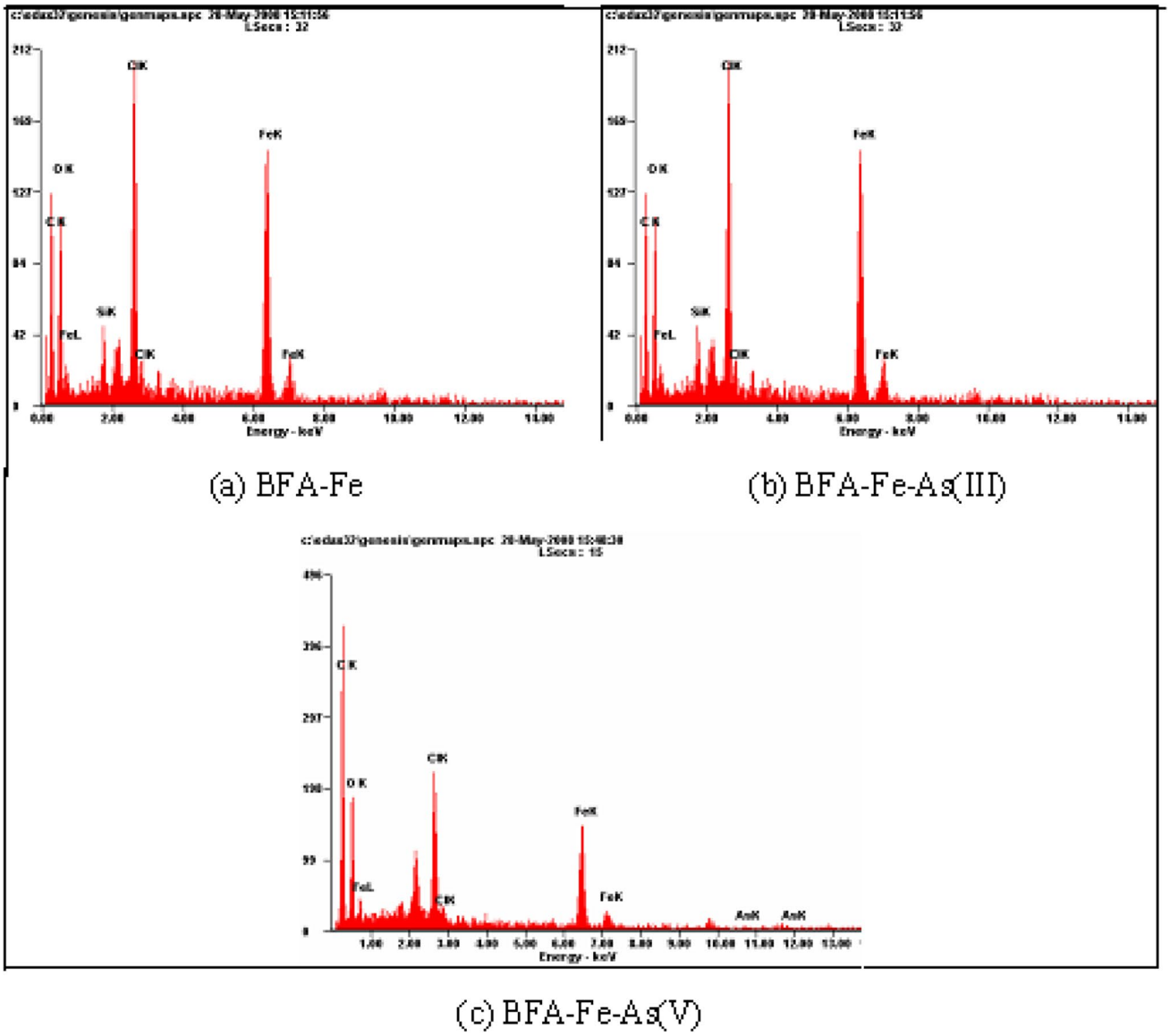

Fig. 3 EDAX spectra analysis of adsorbent before and after adsorption

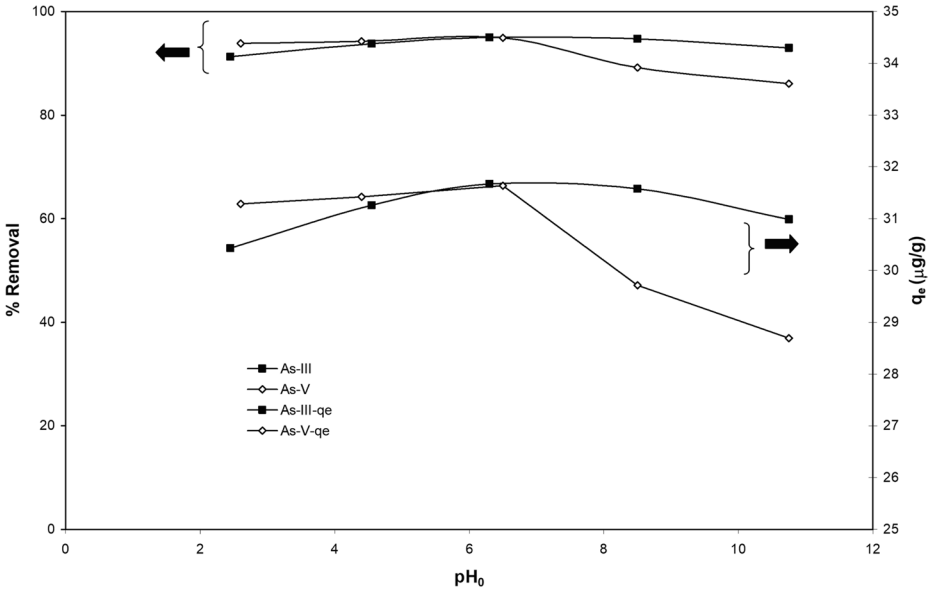

Fig. 4 Effect of initial pH on the equilibrium uptake and % removal of As(III) and As(V) ($C_0 = 100$ µg dm^{-3}, m = 3 g $dm.^{-3}$, $T = 303$ K, $t = 5$ h, RPM = 150)

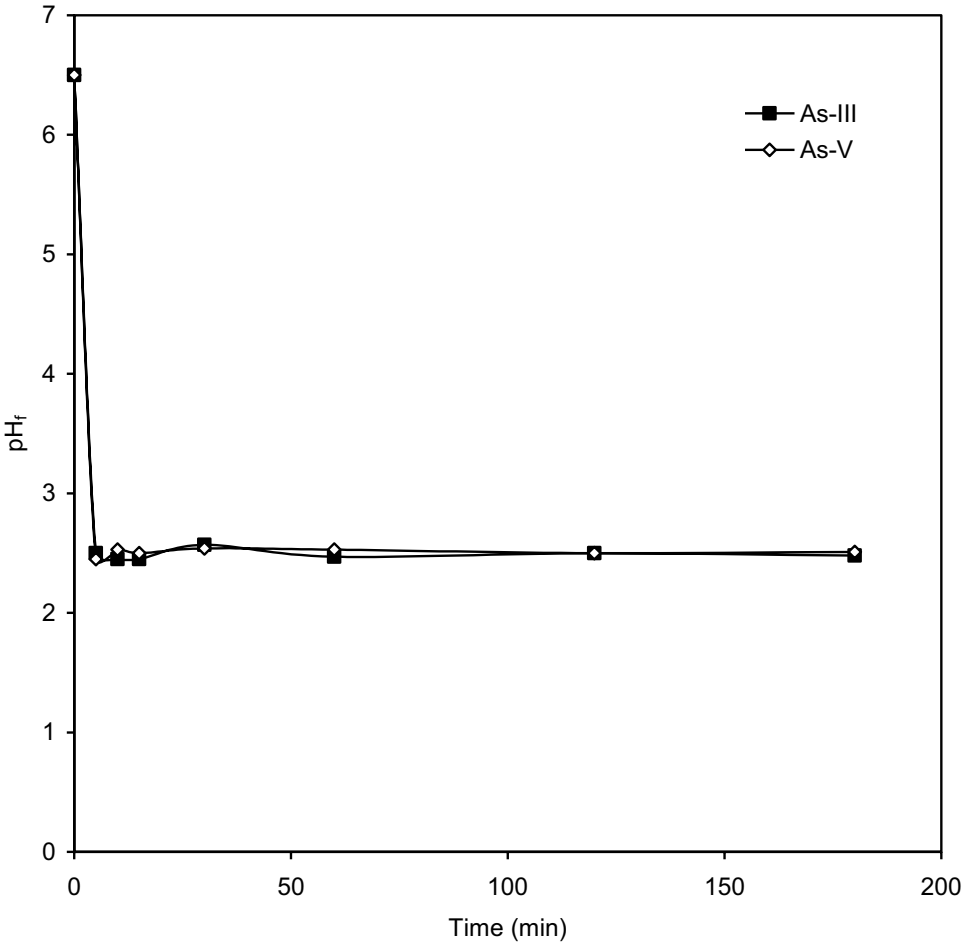

Fig. 5 Change in pH with time after addition of adsorbent (T = 303 K, $C_0 = 100$ µg/dm^3, m = 3 g/$dm.^3$ and $pH_0 = \sim 6$)

Adsorbate

The sodium arsenite (As(III)), and sodium arsenate (As (V)) used as a adsorbate. respectively. An accurate amount of respective compound was weighed and dissolved in Millipore water to prepare stock solutions of 1000 mg/dm^3 of arsenite and arsenate. Analytical grade chemicals are used in this study and ions free distilled water was used for preparing stock solution and required dilution. The analysis of the samples of As (III) and As(V) were done by using a Perkin Elmer, ICP-MS using Elanta software.

Batch adsorption study

The batch adsorpotion study was performed in a 100 ml concial flask with lid. The experimental study was carried with different effects on process affecting parameters such as mass of the BFA-Fe (m), pH_o, temperature, concentration (C_o) of As (III) or As (V) with prospective time (t) in a room atmosphere. The pH was adjusted using either NaOH or HCl. The detailed experimental procedures were reported by Kamsonlian et al. [3–5]. The effect of contact time on the removal was studied by contacting the solution of known concentration and adsorbent dose and the wimples were drawn at particular time interval and were tested for the removal of arsenic. In order to achieve adsorption isotherms of As(III) and As(V), temperature and concentration was varied from 283 to 323 K, and 20–500 µg/dm^3 in a known mass of the BFA-Fe, and 150 rpm speed. The residual As(III) and As(V) concentration (C_e) of the filtrate was then determined. The amount of As(III)/As(V) adsorbed by BFA-Fe at equilibrium was calculated as:

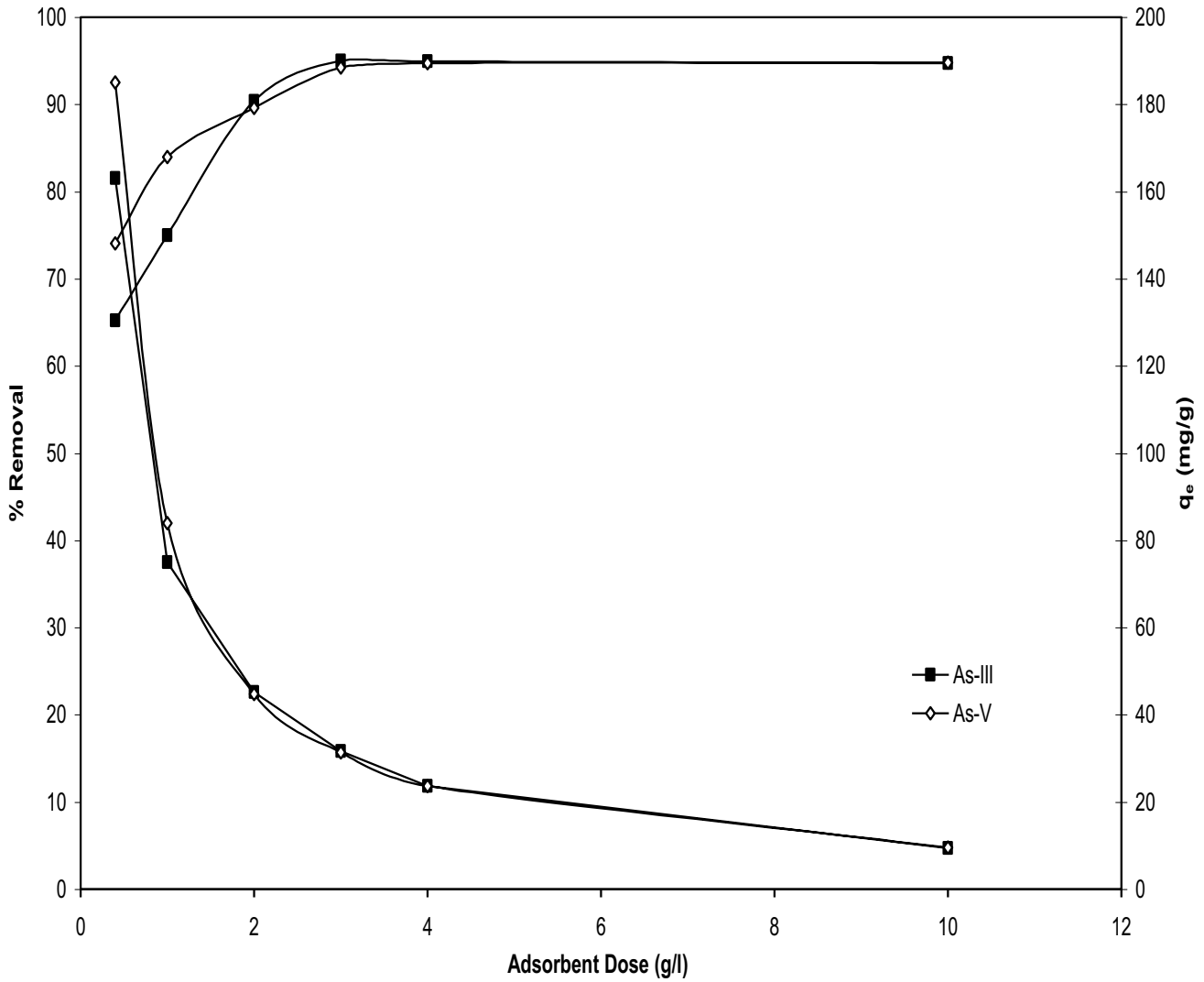

Fig. 6 Effect of BFA-Fe dose on the removal of As(III) and As(V) (C_0 = 100 µg/dm.^{3}, pH_o = 6.3 and 6.5 for As(III) and As(V) respectively, T = 303 K, t = 5 h)

$$q_e = \frac{(C_o - C_e)V}{W} \quad (1)$$

where

C_o and C_e are initial and equilibrium concentrations (μg/dm^3) of As(III) and As(V) in the solution,

V in (dm^3) and

W in (g) of the BFA-Fe.

Regeneration study

Two different batch desorption studies were carried out through chemical solvent, and thermal methods. The detailed procedure was given in elsewhere [48]. The different chemical solvents were agitated with As(III) or As (V)-loaded BFA-Fe (0.2 g). In the thermal regeneration study, the As(III) or As (V)-loaded BFA-Fe was used for thermal desorption study after sufficient dry in an oven followed by furnace. The adsorption–desorption cycles was repeated upto six runs at constant temperature 303 K.

Results and discussion

Characterization of adsorbent

The fractional sieve analysis of the particles of BFA-Fe showed: -600 + 425 mesh size: 31.42%; -425 + 180 mesh size: 58.43%. The fractional sieve analysis of the particles of RHA-Fe showed -600 + 425 mesh size: 35.72%; -425 + 300mesh size: 49.58%; -300 + 180 mesh size: 13.50%. The physical characteristics and elemental composition of the adsorbents are presented in Table 1. BET surface area and pore volume of BFA-Fe was found to be 118.23 m^2/g and 0.3834 cm^3, respectively. Figure 1 shows the SEMs of blank BFA-Fe, and BFA after loading with the arsenic solutions. From the figure of spent BFA-Fe

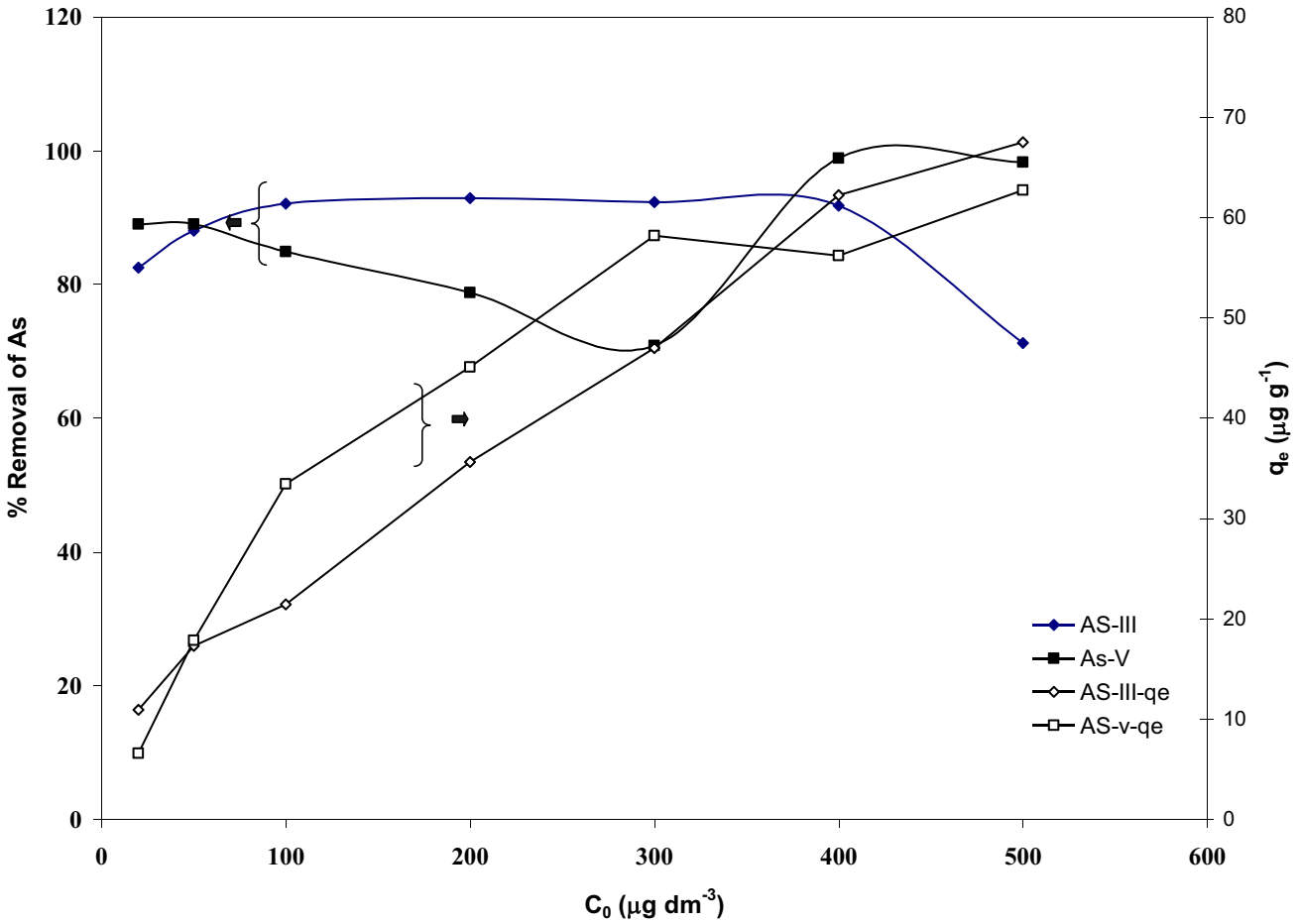

Fig. 7 Effect of initial concentration on the removal of As(III) and As(V), (m = 3 g/dm.^{3}, T = 303 K, pH_0 = Natural (6.3), RPM = 150, Time = 5 h)

shows surface was heterogeneous structure which filled with pores, cracks etc. as compared to the BFA-Fe surface. This is due to adsorption of As on the BFA-Fe surface. Similar observation was reported by Zhu et al. [49] and DhanaRamalakshmi et al. [26] for Fe(III)-sugarcane bagasse and wood carbon-iron oxide composite. EDAX analysis of the adsorbents before and after adsorption was performed to estimate the composition of various elements present in the adsorbents (shown in Fig. 2). The analysis shows the BFA-Fe has more carbon content and has more affinity to impregnate iron as shown by higher content of iron and chloride in BFA-Fe, (Table 2).

Figure 3 FTIR spectra of BFA-Fe and after adsorption of Adsorption of As (III)- and As (V)-BFA-Fe. A intense peaks at 3100 and 3400 cm^{-1} (O–H groups) in both the adsorbents [1–3]. The broad peaks at 3400 cm^{-1} (Si − OH stretching) shows absorbed of water molecules and 1500 cm^{-1} (C-O stretching due to aldehydes and ketones). The peaks were affected due to As-adsorption onto BFA-Fe at 1400 to 1500 cm^{-1} and 1520 to 1550 cm^{-1}. These peaks shifted on adsorbed surface in the present study [25, 40, 49].

In general, adsorption capacity of arsenic is depends on different process affecting parameters mass of the adsorbents, iron concentration, pH, temperature, and treatment time. Many of researchers were explained mechanism of adsorption are resembles with surface complexation, electrostatic attraction, and ion exchange [3–5, 50, 51].

In general, adsorption capacity of arsenic is depends on different process affecting parameters mass of the adsorbents, iron concentration, pH, temperature, and treatment time. Many of researchers were explained mechanism of adsorption are resembles with surface complexation, electrostatic attraction, and ion exchange [50, 51] (Fig. 4).

pH effect on adsorption of As (III) and As (V)

The initial pH effect was studied with As (III), and As (V) solutions of $C_0 = 100$ µg/dm^3 at m = 3 g/dm^3. The solution was kept at 30 ℃ for 5 h, after which the residual concentration of arsenic was determined. The pH of the solution changes to around 2.5 after addition of BFA-Fe in both the cases from the initial pH ~ 6.3–6.5 (shown in Fig. 5). from the figure shows adsorption of As increases with increase of pH upto 6.5 and then slightly decreases on further increase in pH upto 10.5. The final pH obtained here is equal to about the pH_{PZC} which is about 2. In general, the pH of the

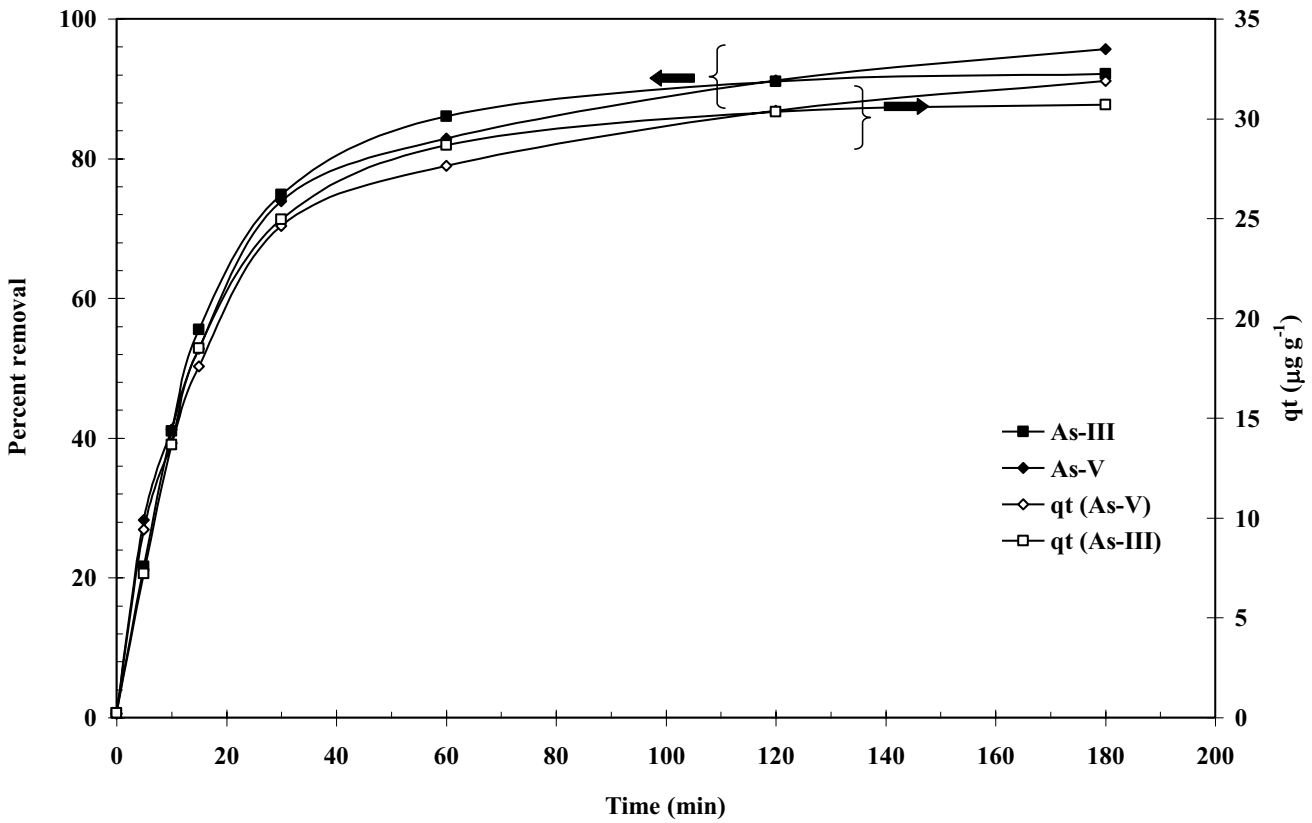

Fig. 8 Time versus Percent Removal plot for the removal of As(III) and As(V) by $T = 303$ K, $C_0 = 100$ µg/dm^3, $m = 3$ g/$dm.^3$, RPM = 150

solution after addition of the adsorbent dose is increases if the pH of the solution pH is less than the point of zero charge and vice-versa. Kamsonlian et al. [5] reported better adsorption in acidic pH of As (V) as compared to basic pH. The maximum removal efficiency found to be at pH 6.3 are ~ 95% and ~ 94%, respectively for As(III) and As(V). This is because of As mainly present in the inorganic form which depends on redox potentials along with solution pH. Bissen et al. [52] reported As (V) oxidation state in environment whereas As (III) is in reducing state which remains uncharged in natural pH. Lobo et al. [53] demonstrated As (V) adsorption onto impregnated chitosan with Iron and found higher efficiency (88.9%) in a pH range of 6 to 9.

Effect of BFA-Fe mass (m)

Figure 6 shows adsorption of As on different mass of BFA-Fe at constant initial concentration of 100 µg/dm^3. It is observed from the figure that arsenic removal is increases from ~ 65% to ~ 94% from 0.4 g/ dm^3 to 3 g/dm^3 adsorbent dosage respectively, for As(III) and after the dose of 3 g/ dm^3 the removal of arsenic is not affected, it remains constant. Similarly, for As(V) the percent removal is increases from ~ 75% to ~ 96% for the above mentioned dose upto 3 g/dm^3. However the adsorption uptake q is found to be decreasing from ~ 163 to ~ 9.5 µg/g for As(III) and from 185 to 9.5 for that of As(V). Beyond the adsorbent dose 3 g/ dm^3 the percent removal is seems to be almost constant, therefore this dose is considered as the optimum adsorbent dose for the removal of arsenic. The increase in the removal of adsorbate with an increase in m for a fixed C_0 can be attributed to the greater surface area and increased number of adsorption sites. Particle–particle interaction may also desorb some of the sorbates that is only loosely and reversibly bound to the adsorbent surface. As adsorption decreased with an increase in C_0. Similar trends of adsorption were found by Zhen [54] onto Fe(III)-Si Binary Oxide Adsorbent. Cooper et al. [42] demonstrated granular activated carbon has poor adsorption of As due to its negative surface charge. However, Muniz et al. [46] and Almazanchez et al. [55] used impregnated granular activated carbon with iron for removal of arsenic and found better adsorption capacity.

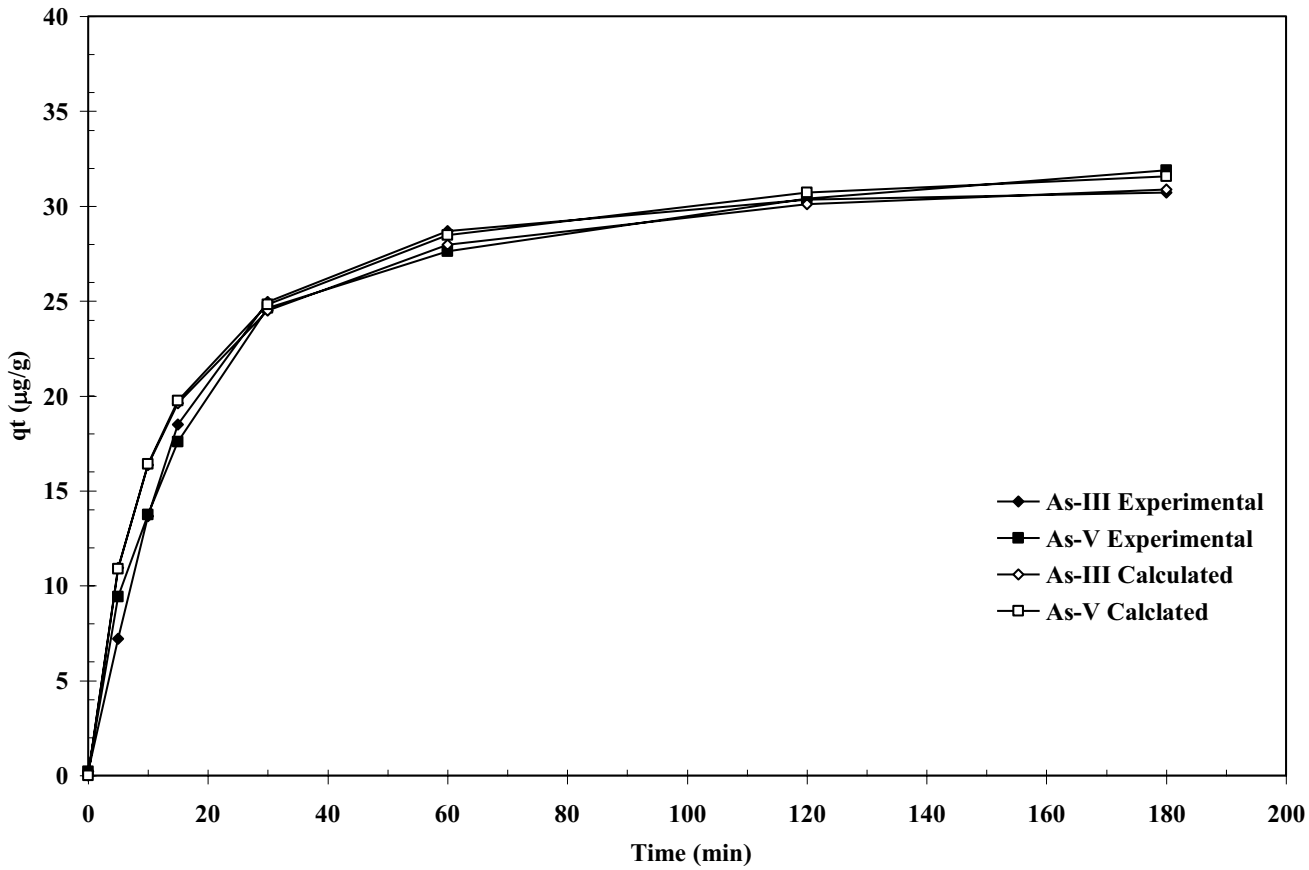

Fig. 9 Time versus q_t (Experimental and Calculated from the pseudo-second order constants) plot for the removal of As(III) and As(V). $T = 303$ K, $C_0 = 100$ µg/dm^3, $m = 3$ g/dm.^{3}

Table 3 Kinetic parameters for the removal of As(III) and As(V)

Models		
Pseudo-first-order	As(III)	As(V)
$q_{e,exp}$ (μg g^{-1})	30.70	31.88
$q_{e,calc}$ (μg g^{-1})	32.55	28.28
k_f (min^{-1})	0.056	0.045
R^2	0.991	0.992
Pseudo-second-order		
$q_{e,calc}$ (μg g^{-1})	32.57	33.37
h (μg g^{-1} min^{-1})	3.250	3.190
k_s(g μg^{-1} min^{-1})	0.0031	0.0029
R^2	0.997	0.999
Intra particle diffusion		
k_{int1}(μg g^{-1} $min^{-1/2}$)	5.90	4.97
C_1(μg g^{-1})	-8.199	-1.8055
R^2	1	0.999
k_{int2} (μg g^{-1} $min^{-1/2}$)	0.591	0.905
C_2 (μg g^{-1})	22.17	20.13
R^2	0.918	0.988
Bangham		
α	0.539	1.342
k_0 (μg^{-1} dm^{-3})	3.990	0.519
R^2	0.553	0.724

Vitelarodriguez and Rangelmendez [56] reported adsorption of As (V) was higher after impregnated granular activated carbon with hematite and akageneite. Deliyanni et al. [57] reported more removal efficiency in the lower concentration of As based adsorption system as compared to the higher concentration of As through iron impregnated granular activated carbon surface. This is due to iron impregnated surface activates different functional groups of carboxy- and hydroxyl ions [58].

Effect of contact time

A short reaction or adsorption times is always achieved in the ideal adsorption processes, i.e. BFA-Fe surface is more adsorb by the As (III) or As (V) in order to attain equilibrium at short period of time. Figures 7 and 8 shows adsorption time on As removal onto BFA-Fe at $C_0 = 100$ μg/dm^3, $m = 3$ g/dm^3, $T = 303$ K, and $pH_0 = 6.3–6.5$. The figure showed the adsorption of arsenic is gradual over a period of 180 min and the residual As concentration after 180 min is ~ 7 μg/dm^3. For BFA-Fe-As system, about 85–87% of As adsorption efficiency in ~ 50 min treatment time and after 50 min, As adsorption is less. The quasi-equilibrium was found to be 3 h. This is normally depends on the properties and

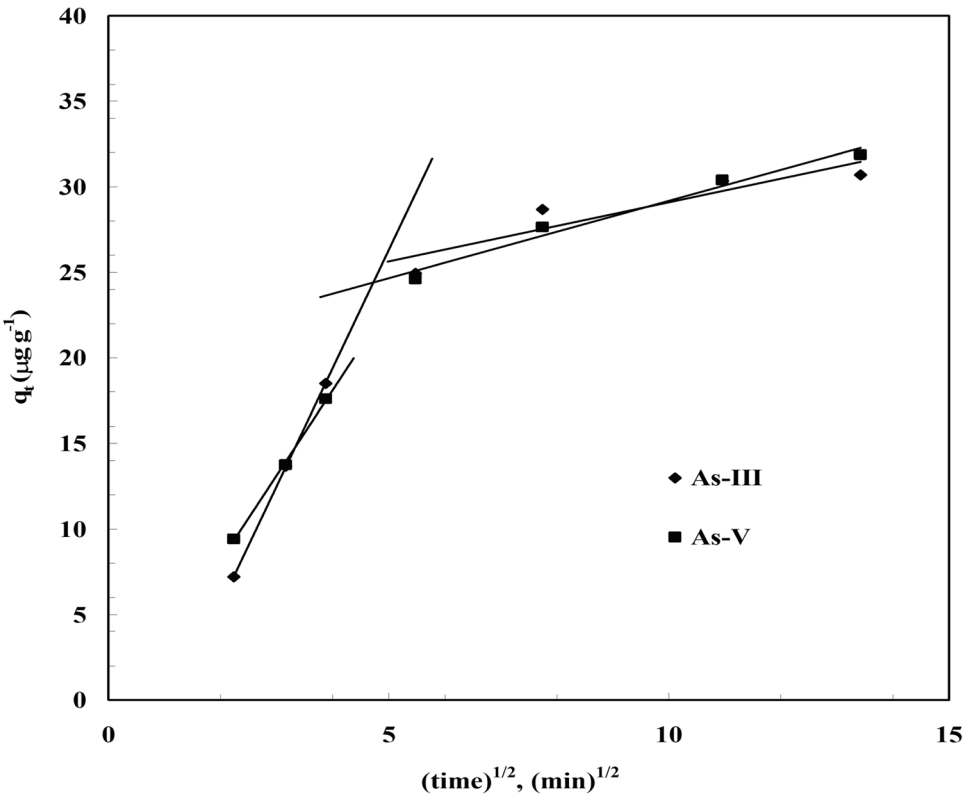

Fig. 10 Weber and Morris intra-particle diffusion plot for the removal of As(III) and As(V). $T = 303$ K, $C_0 = 100$ μg/dm^3, $m = 3$ g/$dm.^3$

nature of adsorbent surface. Wang et al. [59] and Marques Neto, et al. [60] demonstrated adsorption of As (V) onto impregnated chitosan with zerovalent ion, and Fe doped chitosan attain equilibrium after 3 h and 2 h, respectively. Overall adsorption capacity (µg/g) was found to be 33.38 which higher than reported by Ali et al. [61].

Kinetic of As (III), and As (V) adsorption onto BFA-Fe

The fundamental and detailed adsorption kinetic models equation is reported by many researchers [41, 50] which are used to explain the sorption kinetics of As (III), and As (V) onto BFA-Fe. This equation has been solved by using non-linear technique using Microsoft Excel's solver-add-in for obtaining constants function. Figure 9 shows kinetic plot of As adsorption onto BFA-Fe at maintained constant process conditions, $C_0 = 100$ µg/dm^3, 30^{0}C, pH_0: 6.3–6.5, and m = 3 g/dm^3. The correlation coefficients (R^2) are obtained from kinetic plot which shown in Table 3. From the table shows R^2 values are 0.991, 0.992, and 0.997, 0.999 for As (III), and As (V) pseudo-first-order, pseudo-second-order, respectively. It shows that pseudo-second-order is best fitted for both of As kinetic datas as compared to pseudo-first-order. It is also shows that rate follows chemical or activated mechanical adsorption mechanism [60]. Similar conclusion were drawn for adsorption of As (V) onto impregnated chitosan with Iron, clay, magnetite, molybdate oxoanions, egg shell [53, 62–64]. Figure 10 shows a representative q_t versus $t^{0.5}$ plot for As(III) and As(V) onto BFA-Fe for C_0= 100 µg/dm^3 at 303 K and pH_0 6.3–6.5. From Fig. 11 it can be seen that pore diffusion is the controlling-step during the adsorption of As onto BFA-Fe. Figure 12 shows a representative plots of $\text{loglog}\left(C_O/\left(C_O - q_t m\right)\right)$ versus log(t) plot for As adsorption onto BFA-Fe for C_0= 100 µg/dm^3 at 303 K and at pH_0 6.3–6.5. However, the plot (Fig. 12) according to above equation did not yield linear curves and the values of R^2 are far from one. The values of effective diffusivity coefficient D_e (m^2/s) of various adsorbate-adsorbent system by vermeulen's equation (shown in Fig. 13). Effective pore diffusivities of As(III) and As(V) was found to be 7.95×10^{12} and 4.89×10^{12}, respectively. This shows that As(III) have highest overall pore diffusion rate.

Adsorption equilibrium modelling

Figures 13 and 14 shows isotherms plots for the adsorption of As onto BFA-Fe with different temperature and found that the temperature increases with As adsorption increased.

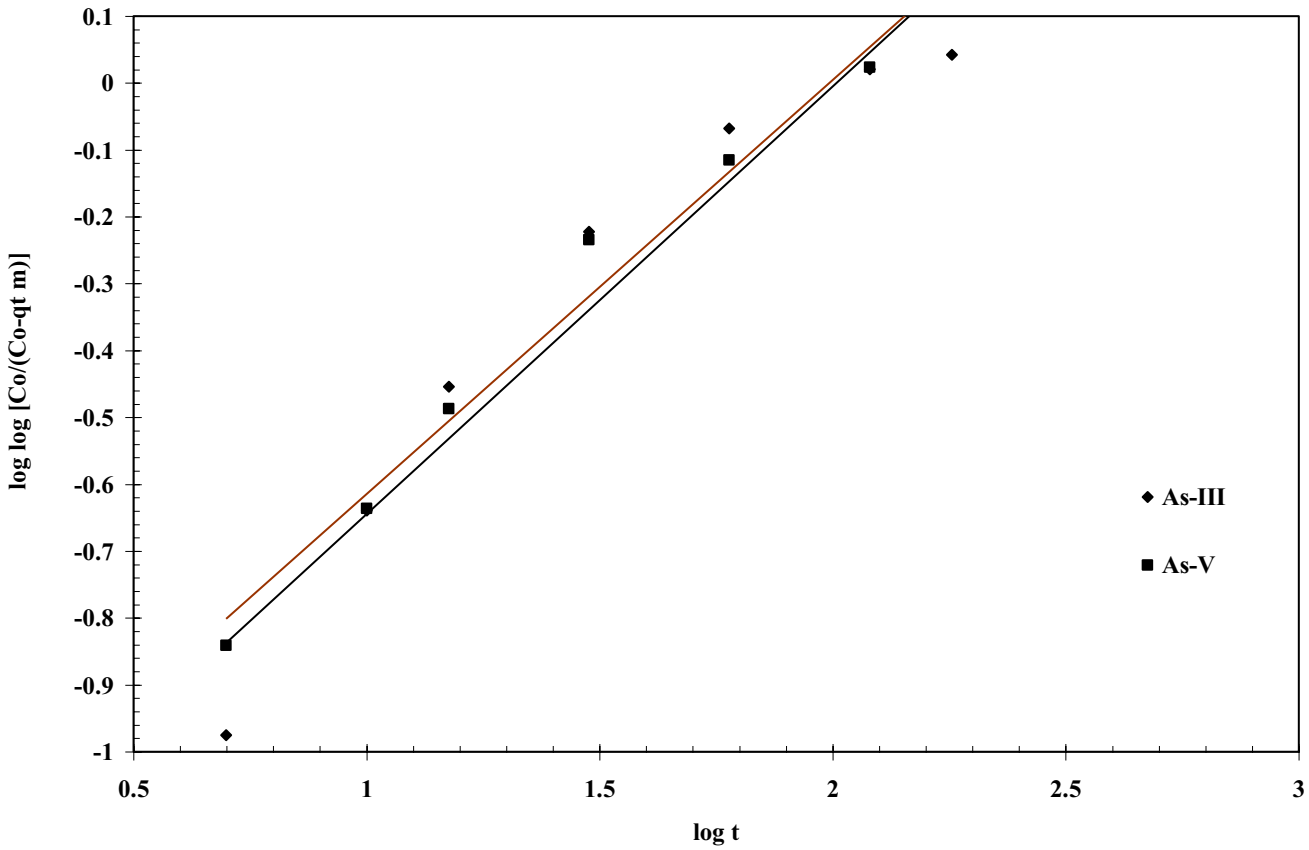

Fig. 11 Bangham plot for the removal of As(III) and As(V). $T = 303$ K, $C_0 = 100$ µg/dm^3, $m = 3$ g/dm.^{3}

From this results revealed that exothermic process follows for adsorption of As (II), and As (V) onto BFA-Fe. The different models are fitted with experimental datas [65–68]. The detailed description of the models equation are given in elsewhere [41]. The isotherms constants obtained by non-linear regression analysis using MS Excel are given in Tables 4 and 5. The different error functions was used to solve non-linear equations such as HYBRID, MPSD, SSE, SAE, and ARE which can represent the suitability for data obtained during adsorption process. For Freundlich isotherm, found from Table 5, that the BFA showed greater heterogeneity for As-III than that of for other adsorbate-adsorbent systems. Since for all the adsorbates, $1/n < 1$, the adsorbates are favourably adsorbed by BFA. Table 6 shows values of error interpretation on experimental data, R-P isotherm best represent the equilibrium adsorption of As on BFA-Fe. Almazanchez et al. [55] reported isotherm data is best fitted by using R-P model for adsorption of As on impregnated granular activated carbon with iron oxide.

A classical Van't Hoff equation was used for determining Gibbs free energy change ΔG^0_{ads} of the adsorption process (shown in Fig. 15) and estimated values of ΔH^0 and ΔS^0 shown in Table 7. ΔG^0_{ads} should be negative value for adsorption process at any process temperature (283 K to 323 K). For R-P model, the value found to be -43.85, -45.34, -48.82, -51.31, -53.8, and -44.75, -48.3, -51.84, -55.39, -58.93, -55.57 for As (III), and As (V), respectively at 283 K, 293 K, 303 K, 313 K, 323 K. The negative values of ΔH^0 shows exothermic in nature.

Thermal degradation kinetics of the spent BFA-Fe and regeneration studies

The disposal of spent adsorbents is a major environmental problem. The chemical and thermal methods was performed to regenerate adsorbed As in the spent BFA-Fe As(III), and As (V) surface which is more important while designing the adsorption column in the large scale. This can reduce both cost process and operation as well as helps to reuse for material persist to the other application, if suits. For solvent regeneration, As(III) or As (V) loaded BFA-Fe shown in Fig. 16a. Among the various solvents, only all acid solvents such as HCl, H_2SO_4 and HNO_3 were found to be a better elutant for desorption of loaded BFA-Fe.

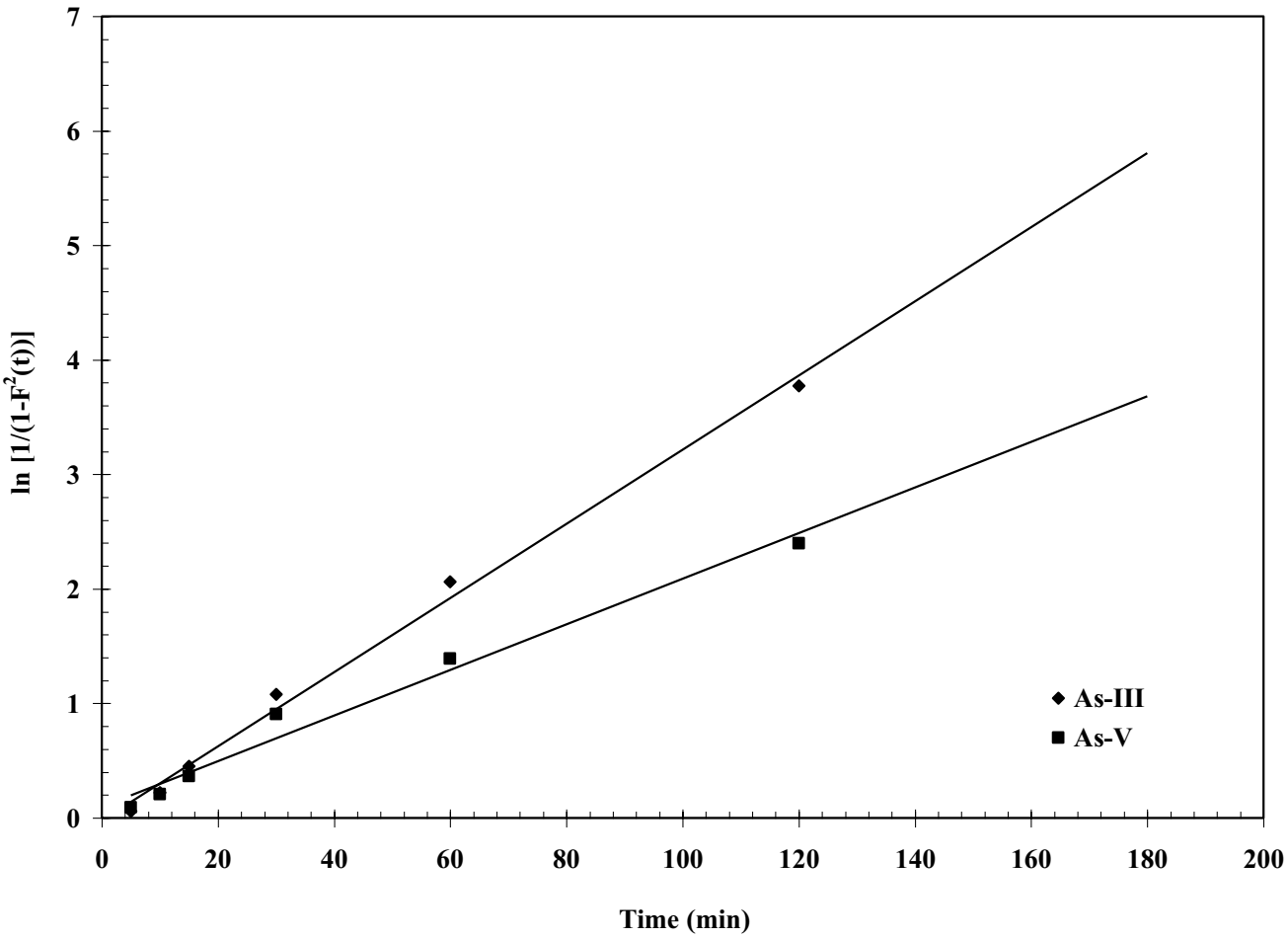

Fig. 12 F(t) plot for the determination of effective pore diffusivity (D_e) of As(III) and As(V). $T = 303$ K, $C_0 = 100$ µg/dm^3, $m = 3$ g/dm.^{3}

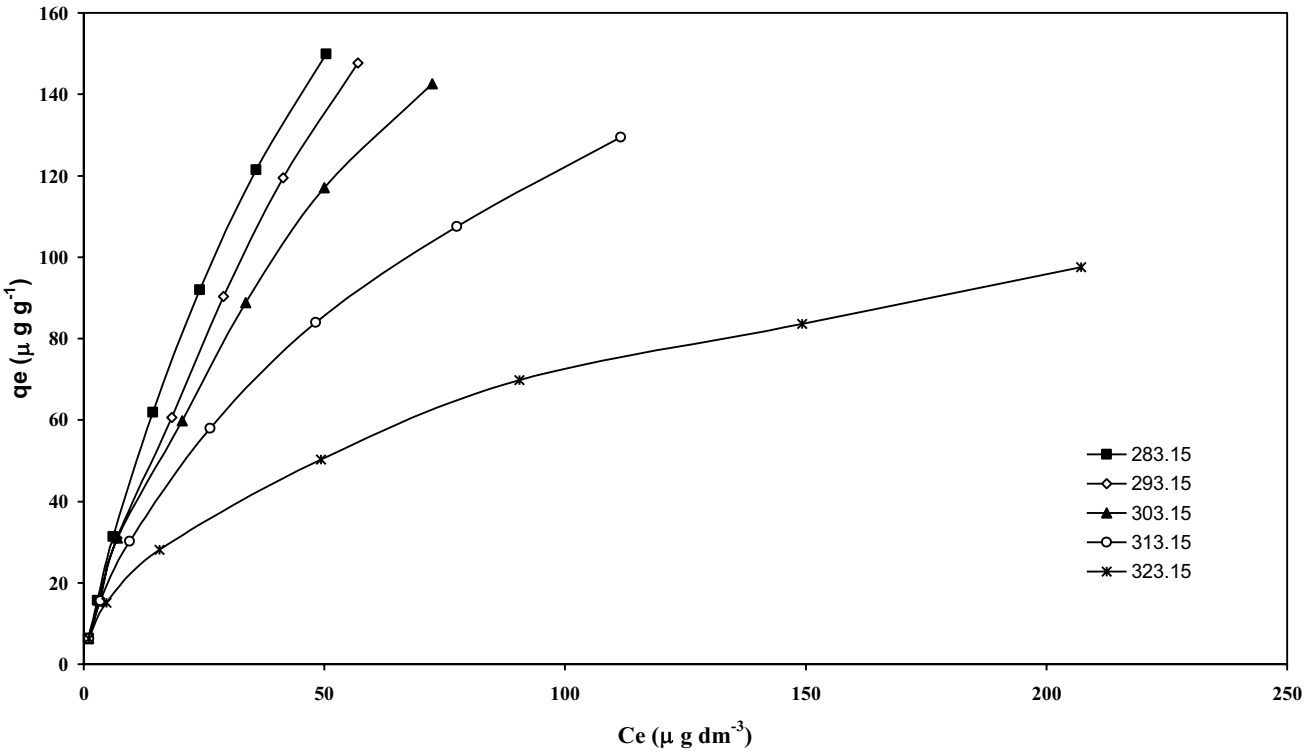

Fig. 13 Equilibrium adsorption isotherms at different temperatures for adsorption of As(III). ($pH_0 = 6.3$, $C_0 = 20–500$ μg/dm^3, $m = 3$ g/dm.^{3})

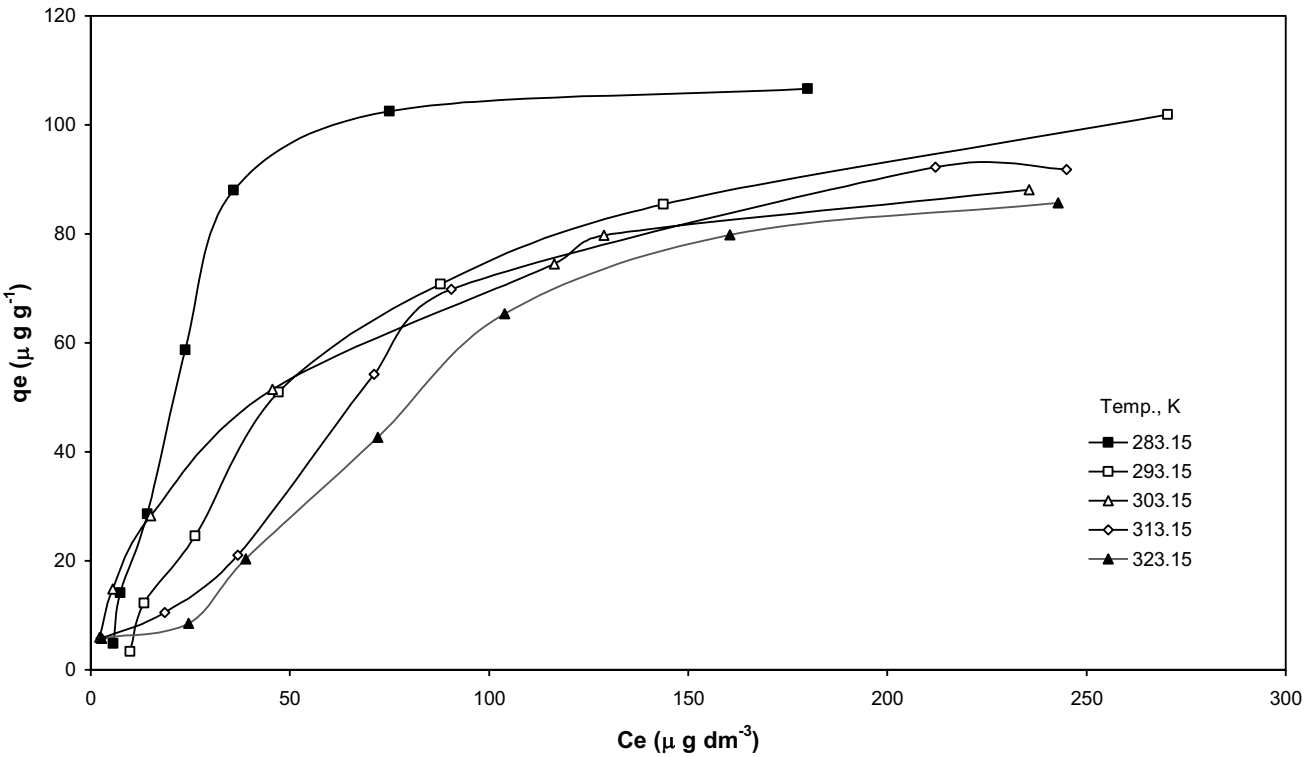

Fig. 14 Equilibrium adsorption isotherms at different temperatures for adsorption of As(V). ($pH_0 = 6.5$, $C_0 = 20–500$ μg/dm^3, $m = 3$ g/dm.^{3})

Table 4 Isotherm parameters for the adsorption of As(III) onto BFA-Fe at different temperatures

Isotherms	Constants	Temperatures (Kelvin, K)				
		283	293	303	313	323
Langmuir	K_L, $dm^3\ \mu g^{-1}$	0.034	0.008	0.245	0.018	0.002
	q_m, $\mu g\ g^{-1}$	109.890	144.928	13.514	217.391	553.595
	R^2 (dm^3 linear)	0.932	0.951	0.991	0.997	0.993
	R^2 (Non-Linear)	0.984	0.997	0.999	0.998	0.997
	HYBRID	-1.885	-3.029	93.757	-0.218	-123.732
	MPSD	12.153	5.025	81.154	4.092	150.113
Freundlich	K_F, $dm^3\ \mu g^{-1}$	8.209	1.833	5.948	7.050	3.248
	n	1.883	1.314	1.511	1.513	1.802
	1/n	0.531	0.751	0.521	0.551	0.555
	R^2 (Linear)	0.891	0.984	0.952	0.953	0.955
	R^2 (Non-Linear)	0.944	0.992	0.981	0.981	0.978
	HYBRID	-1.545	-0.933	-1.571	-1.570	5.724
	MPSD	19.045	13.718	17.199	18.232	20.277
Temkin	B	25.475	23.579	25.139	39.938	11.857
	K_T, $dm^3\ \mu g^{-1}$	0.275	0.152	0.323	0.253	0.394
	R^2 (Linear)	0.913	0.957	0.977	0.953	0.971
	R^2 (Non-Linear)	0.955	0.978	0.989	0.981	0.985
	HYBRID	-2.353	20.414	7.047	13.215	22.194
	MPSD	10.855	75.181	33.357	50.847	58.844
Redilich-Peterson	a_R, $dm^3\ \mu g^{-1}$	1.742	5.758	1.410	1.573	20.547
	K_R, $dm^3\ \mu g^{-1}$	8.400	12.000	12.292	15.805	58.723
	B	0.559	0.255	0.415	0.394	0.450
	R^2 (Linear)	0.887	0.853	0.782	0.889	0.934
	R^2 (Non-Linear)	0.942	0.877	0.884	0.942	0.955
	HYBRID	108.144	-1.001	-1.405	-1.551	2.239
	MPSD	82.139	14.977	22.324	18.315	33.301

Table 5 Isotherm parameters for the adsorption of As(V) onto BFA-Fe at different temperatures

Isotherms	Constants	Temperatures (Kelvin, K)				
		283	293	303	313	323
Langmuir	K_L, $dm^3\ \mu g^{-1}$	0.005	0.007	0.011	0.014	0.011
	q_m, $\mu g\ g^{-1}$	555.555	133.333	357.143	81.957	115.279
	R^2 (Linear)	0.701	0.904	0.845	0.978	0.872
	R^2 (Non-Linear)	0.837	0.951	0.921	0.989	0.934
	HYBRID	-53.388	58.381	-2.371	4.148	5.250
	MPSD	47.282	50.771	19.200	15.785	28.029
Freundlich	K_F, $dm^3\ \mu g^{-1}$	2.121	3.255	4.495	2.527	2.940
	n	1.059	1.405	1.172	1.504	1.542
	1/n	0.935	0.712	0.853	0.524	0.548
	R^2 (Linear)	0.987	0.981	0.955	0.987	0.995
	R^2 (Non-Linear)	0.993	0.980	0.978	0.994	0.993
	HYBRID	-0.884	-0.928	-3.721	-0.905	3.138
	MPSD	12.378	13.595	27.511	11.772	23.757
Temkin	B	45.278	22.252	48.904	13.810	15.800
	K_T, $dm^3\ \mu g^{-1}$	0.154	0.271	0.314	0.305	0.280
	R^2 (Linear)	0.908	0.889	0.945	0.919	0.833
	R^2 (Non-Linear)	0.953	0.943	0.973	0.959	0.913
	HYBRID	25.703	15.775	53.709	-385.128	25.534
	MPSD	80.909	85.552	170.095	485.235	83.789
Redilich-Peterson	a_R, $dm^3\ \mu g^{-1}$	20.359	0.851	3.020	11.830	251.548
	K_R, $dm^3\ \mu g^{-1}$	45.233	5.375	15.745	31.712	759.723
	B	0.057	0.911	0.138	0.385	0.352
	R^2 (Linear)	0.251	0.757	0.254	0.958	0.998
	R^2 (Non-Linear)	0.990	0.984	0.994	0.990	0.999
	HYBRID	-0.737	-0.402	-8.184	-0.755	4.014
	MPSD	13.780	20.392	32.584	12.771	20.559

Table 6 Error analyses functions for adsorption of As(III) and AS(V) onto BFA-Fe

Temperature(K)/ Isotherms	As(III)					As(V)				
	HYBRID	MPSD	SSE	SAE	ARE	HYBRID	MPSD	SSE	SAE	ARE
Langmuir										
283	-1.89	12.15	229.41	31.05	57.79	-53.39	47.28	351.54	123.55	38.14
293	-3.03	5.03	219.89	5.35	42.99	58.38	50.77	253.40	115.18	41.7
303	93.75	81.15	192.53	22.30	55.97	-2.37	19.20	291.84	30.17	12.57
313	-0.22	4.09	379.58	13.19	42.95	4.15	15.78	25.12	12.37	9.05
323	-123.73	150.11	398.98	350.92	95.11	5.25	28.03	853.55	52.75	19.19
Freundlich										
283	-1.55	19.04	959.93	59.53	13.21	-0.88	12.38	931.39	48.77	9.12
293	-0.94	13.72	147.50	25.44	10.20	-0.92	13.59	407.95	39.45	10.22
303	-1.57	17.20	778.74	47.72	12.51	-3.72	27.51	445.00	100.10	19.00
313	-1.57	18.23	977.48	72.42	72.42	-0.90	11.77	155.20	24.24	8.40
323	5.72	20.27	87.50	19.93	13.45	3.14	23.75	172.95	48.08	11.35
Temkin										
283	-2.37	10.85	317.15	33.81	7.34	25.70	80.90	1345.22	90.32	47.34
293	20.41	75.18	245.85	38.75	35.91	15.77	85.55	559.73	55.38	44.99
303	7.05	33.35	145.50	25.37	15.59	53.71	170.09	1545.40	90.77	71.75
313	13.21	50.85	555.53	55.95	24.40	-385.12	485.23	1588.80	340.37	75.80
323	22.19	58.84	320.40	37.58	30.12	25.53	83.79	801.05	59.39	42.52
Redlich-Peterrson										
283	8.14	82.14	128.90	275.41	51.80	-0.73	13.78	905.05	48.51	48.51
293	-1.00	14.98	143.72	25.05	9.99	49.40	40.39	1287.90	74.52	28.23
303	-1.40	22.32	177.30	53.05	12.02	-8.18	32.58	8314.44	122.51	19.35
313	-1.55	18.31	159.85	57.13	12.03	-0.77	12.77	145.70	23.57	8.15
323	2.24	33.30	755.41	50.32	24.45	4.01	25.57	1173.57	48.10	11.37

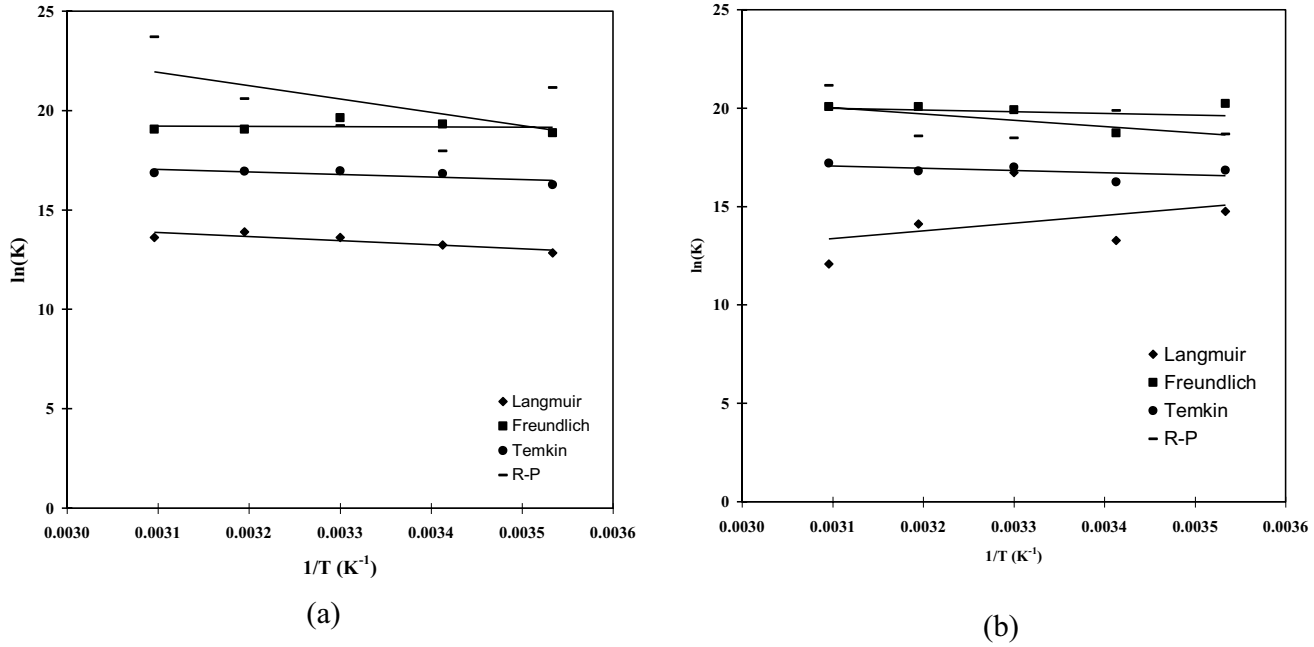

Fig. 15 Van't Hoff plot for the adsorption of (**a**) As (III), and (**b**) As (V) onto BFA-Fe

Table 7 Thermodynamic parameters for the sorption of As(III) and As(V) onto BFA-Fe

Compounds	ΔG^0_{ads}(KJ mol^{-1})					ΔH^0(KJ mol^{-1})	ΔS^0(KJ mol^{-1} K^{-1})
	283 K	293 K	303 K	313 K	323 K		
Langmuir							
As(III)	-35.47	-35.57	-35.57	-35.78	-35.88	-32.55	0.01
As(V)	-30.53	-32.21	-33.9	-35.58	-37.27	-17.19	0.17
Freundlich							
As(III)	-45.14	-48.04	-49.93	-51.82	-53.71	-7.39	0.19
As(V)	-44.72	-47.01	-49.31	-51.5	-53.89	-20.119	0.23
Temkin							
As(III)	-38.97	-40.58	-42.39	-44.09	-45.08	-9.35	0.17
As(V)	-38.81	-40.54	-42.28	-44.01	-45.75	-10.328	0.17
Redilich-Peterson							
As(III)	-43.85	-45.34	-48.82	-51.31	-53.8	-25.58	0.25
As(V)	-44.75	-48.3	-51.84	-55.39	-58.93	-55.57	0.35

Maximum desorption efficiency of As (III) and As (V) were found to be 83.23%, and 73.6%, respectively in HCl. This may be due to stronger surface interaction with the As (III) and As (V). Soltani et al. [24] observed similar desorption of As (V) using HCl reagent onto spent Fe_3O_4/bone char and found < 20% reduction in the efficiency of As (V) removal within three repeated runs. The desorption was least from base solvents due to different factors, polarity, chemical repletion behaviour between base solvents, BFA-Fe and As (III) or As (V), which control desorption efficiency. The thermal regeneration needed subsequent to remove removing As (III) or As (V). Figure 16b shows 6 cycles of thermal adsorption–desorption on spent BFA-Fe which was carried out in a furnace. From the figure, clearly shows after 1st run, thermal desorption decreased with respect to adsorption–desorption cycles. It also shown in literatures [5, 48].

Figure 17a-c shows thermal degradation of BFA-Fe, and spent BFA-Fe surfaces through thermal analysis kept constant flow rate 200 ml/min and 100 ^{0}C/min heat rate. Figure 17a shows thermal stability of BFA-Fe surface which is mainly dependent on the temperature for decomposition into oxides and different functional groups. Initially, moisture content or water molecules evaporated at < 150^{0}C followed by carbon start to decompose at greater than 200^{0}C. During carbon decomposition, CO, CO_2, and free hydrogen produces in the temperature range of 150–500 ^{0}C, 350-1000^{0}C, and 500-1000^{0}C, respectively [5]. From the Fig. 17a, we observed three thermal zones which are room temperature to 400^{0}C, 400^{0}C to 750^{0}C, and 750 ^{0}C to 1000^{0}C, respectively. The weight loss in the first thermal zone was ~ 19% and second thermal zone, maximum weight loss of ~ 35% (2.14 mg/min) was found and third thermal zone shows degradation is negligible amount. We observed from Fig. 17b-c, all the three thermal zones, temperature and weight loss were shifted due to As present in the spent BFA-Fe surface. For example, from the DTA curve, 385^{0}C, 390^{0}C, and 400^{0}C respective for BFA-Fe, BFA-As (III), and BFA-As (V). Our results revealed that BFA-Fe can be reused directly for making fire-briquettes to explore its energy value.

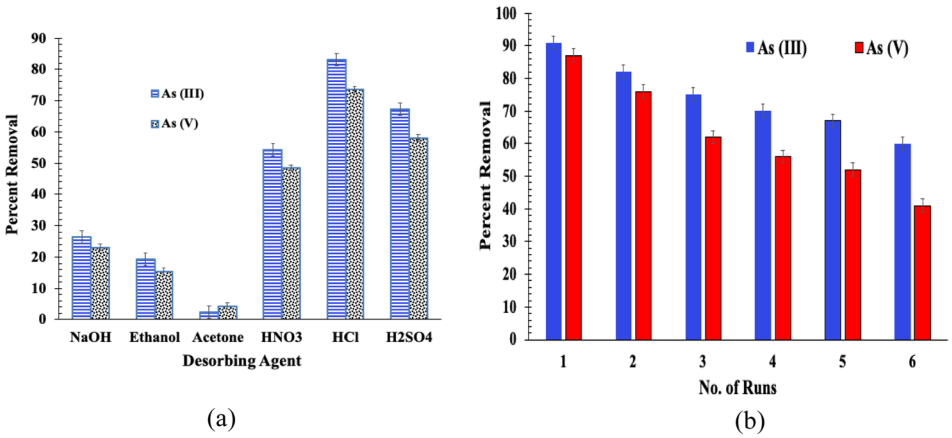

Fig. 16 (**a**) Chemical and (**b**) thermal regeneration of spent BFA-Fe

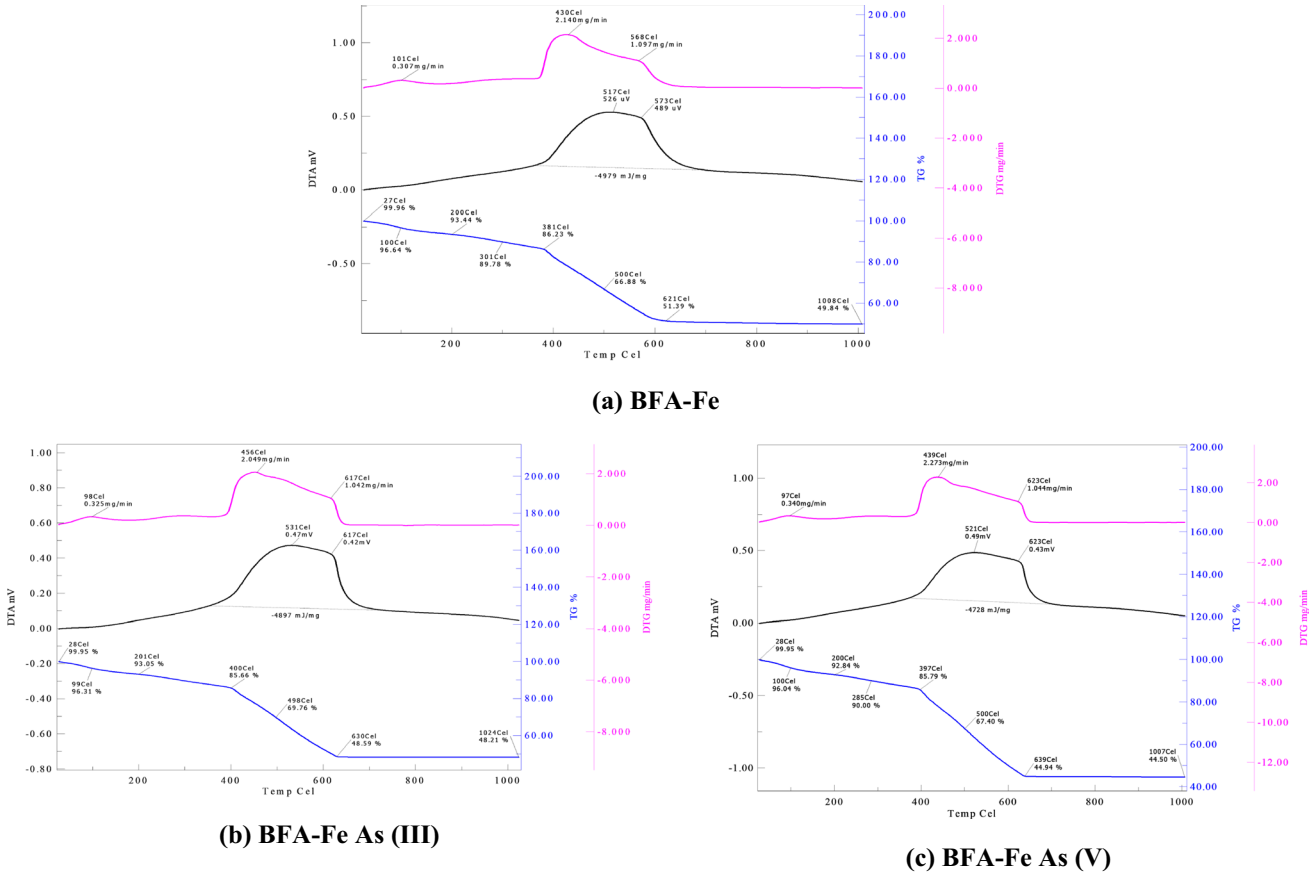

(a) BFA-Fe

(b) BFA-Fe As (III)

(c) BFA-Fe As (V)

Fig. 17 TGA-DTA degradation curve of BFA-Fe surface, and after adsorbed surface of As (III), and As (V)

Conclusion

In this study, adsorption of As (III) and As (V) onto BFA impregnated iron in a water mixture. The EDAX analysis of BFA-Fe showed that has higher carbon and iron content as compared to that of RHA. The FTIR spectra of the adsorbents indicated the presence of various types of functional groups e.g. free and hydrogen bonded OH group, the silanol groups (Si–OH), CO group stretching from aldehydes and ketones on the surface of adsorbents. Optimum BFA and RHA dosages were found to be 3 g/dm^3. The effect of contact on removal shows that the adsorption of As on BFA-Fe is very fast. R-P equation was found to best represent the equilibrium data. An increase in temperature induces a positive effect on the sorption process.Thermodynamic studies revealed that the adsorption of arsenic (As(III) and As(V)) on BFA is exothermic in nature.

Maximum desorption efficiency of As (III) and As (V) were found to be 83.23%, and 73.6%, respectively in HCl. The thermal adsorption–desorption cycles show that spent BFA-Fe was good enough for reuse. Thermogravimetric analysis exhibited the thermal stability of the adsorbents upto 400 °C. The negative value of change in ΔG^0_{ads} indicated the feasibility and spontaneity of adsorption on the adsorbents. It is suggested that the BFA-Fe could be centriclarified from the solution, dried and admixed with bagasse, and reused directly for making fire-briquettes to explore its energy value.

Declarations

Conflict of interest The authors declare that they have no conflict of interest.

References

1. UNICEF report, Safe Drinking Water http://www.unicef.org/specialsession/about/sgreport.pdf/03_SafeDrinkingWaterD7341Insert_English.pdf, cited on 10th June 10, 2019.
2. Mohan D, Pittman JCU. Arsenic removal from water/wastewater using adsorbents—A critical review. J Hazard Mater. 2007;142:1–53.
3. Kamsonlian S, Suresh S, Majumder CB, Chand S. Bio-sorptive behaviour of mango leaf powder and rice husk for arsenic (III) from aqueous solutions. Int J Environ Sci Technol. 2012;9:565–78.

4. Kamsonlian S, Suresh S, Majumder CB, Chand S. Biosorption of arsenic from contaminated water onto solid psidium guajava leaf surface: equilibrium, kinetics, thermodynamics, and desorption study. Bioremed J. 2012;16(2):97–112.
5. Kamsonlian S, Suresh S, Majumder CB, Chand S. Biosorption of As(III) from contaminated water onto low cost palm bark biomass. Int J Current Eng Technol. 2012;2(1):153–8.
6. Yadav SK, Ramanathan A, Kumar M, Chidambaram S, Gautam Y, Tiwari C. Assessment of arsenic and uranium co-occurrences in groundwater of central Gangetic Plain, Uttar Pradesh, India. Environ Earth Sci. 2020;79(6):1–14.
7. Sanyal T, Bhattacharjee P, Bhattacharjee S, Bhattacharjee P. Hypomethylation of mitochondrial D-loop and ND6 with increased mitochondrial DNA copy number in the arsenic-exposed population. Toxicology. 2018;408:54–61.
8. Shaheen SM, Niazi NK, Hassan NE, Bibi I, Wang H, Tsang DC, Ok YS, Bolan N, Rinklebe J. Wood-based biochar for the removal of potentially toxic elements in water and wastewater: a critical review. Int Mater Rev. 2019;64(4):216–47.
9. Amen R, Bashir H, Bibi I, Shaheen SM, Niazi NK, Shahid M, Hussain MM, Antoniadis V, Shakoor MB, Al-Solaimani SG, Wang H, Bundschuh J, Rinklebebk J. A critical review on arsenic removal from water using biochar-based sorbents: the significance of modification and redox reactions. Chem Eng J 2020;396:125195.
10. U.S.E.P.A. (USEPA), Arsenic, Inorganic (CASRN 7440–38–2). Integrated Risk Informa- tion System (IRIS) U.S. , Environmental Protection Agency Chemical, Assessment Summary, National Center for Environmental Assessment, 1998.
11. WHO. Guidelines for drinking-water quality. World Health Organization 2011;216:303–304.
12. Chen Y, Gamble PM, Islam T, Ahmed A, Argos M, Graziano JH, Ahsan H. Arsenic exposure at low-to-moderate levels and skin lesions, arsenic metabolism, neurological functions, and biomarkers for respiratory and cardiovascular diseases: review of recent findings from the Health Effects of Arsenic Longitudinal Study (HEALS) in Bangladesh. Toxicol Appl Pharmacol. 2009;239(2):184–92.
13. Tsuji JS, Garry MR, Perez V, Chang ET. Low-level arsenic exposure and develop- mental neurotoxicity in children: a systematic review and risk assessment. Toxicology. 2015;337:91–107.
14. Lynch HN, Zu K, Kennedy EM, Lam T, Liu X, Pizzurro DM, Loftus CT, Rhomberg LR. Quantitative assessment of lung and bladder cancer risk and oral expo- sure to inorganic arsenic: meta-regression analyses of epidemiological data. Environ Int. 2017;106:178–206.
15. Podgorski J, Berg M. Global threat of arsenic in groundwater. Science. 2020;368:845–50.
16. Kumarathilaka P, Seneweera S, Ok YS, Meharg AA, Bundschuh J. Mitigation of arsenic accumulation in rice: an agronomical, physico-chemical, and biological approach–A critical review. Crit Rev Environ Sci Technol. 2020;50(1):31–71.
17. Kumar M, Ramanathan A. Arsenic speciation of groundwater and agricultural soils in central Gangetic basin, India, p. 225, CRC Press. 2019.
18. Bureau of Indian Standards (BIS), IS 10500 : Drinking water Specification. 2012; 18.
19. Chakrabarti D, Singh S, Rashid M, Rahman MM, Arsenic: Occurrence in Ground- water, Encyclopedia of Environmental Health, 2nd Edtion Elsevier Inc, 2018.
20. Borho M, Wilderer P. Optimized removal of arsenate(III) by adaptation of oxidation and precipitation processes to the filtration step. Water Sci Technol. 1996;34:25–31.
21. Han B, Runnells T, Zimbron J, Wickramasinghe R. Arsenic removal from drinking water by flocculation and microfiltration. Desalination. 2002;145:293–8.
22. Singh TS, Pant KK. Equilibrium, kinetics and thermodynamic studies for adsorption of As(III) on activated alumina. Sep Purif Technol. 2004;36:139–47.
23. Chang YY, Song K, Yang Y. Removal of As(III) in a column reactor packed with iron-coated sand and manganese-coated sand. J Hazard Mater. 2008;150:565–72.
24. Soltani RDC, Safari M, Maleki A, Rezaee R, Shahmoradi B, Shahmohammadi S, Ghahramani E. Decontamination of arsenic(V)-contained liquid phase utilizing Fe_3O_4/bone char nanocomposite encapsulated in chitosan biopolymer. Environ Sci Poll Res. 2017;24:15157–66.
25. Hayati B, Maleki A, Najafi F, Gharibi F, McKay G, Gupta VK, Puttaiah SH, Marzban N. Heavy metal adsorption using PAMAM/CNT nanocomposite from aqueous solution in batch and continuous fixed bed systems. Chem Eng J. 2018;346:258–70.
26. DhanaRamalakshmi R, Murugan M, Jeyabal V. Arsenic removal using Prosopis spicigera L. wood (PsLw) carbon–iron oxide composite. Appl Water Sci. 2020;10:211.
27. Yin Y, Zhou T, Luo H, Geng J, Yu W, Jiang Z. Adsorption of arsenic by activated charcoal coated zirconium-manganese nanocomposite: performance and mechanism. Colloids Surf A. 2019;575:318–28.
28. Dutta PK, Pehoen So, Sharma VK, Ray AK. Photocatalytic oxidation of Arsenic(III): evidence of hydroxyl radicals. Environ Sci Technol. 2005;39:1827–34.
29. Basha CA, Selvi SJ, Ramasamy E, Chellammal S. Removal of arsenic and sulphate from the copper smelting industrial effluent. Chem Eng J. 2008;141:89–98.
30. Ballinas ML, Miguel ERDS, Rodriguez MTJ, Silva O, Munoz M, Gyves JD. Arsenic(V) removal with polymer inclusion membranes from sulfuric acid media using DBBP as carrier. Environ Sci Technol. 2004;38:886–91.
31. Gholami MM, Mokhtari MA, Aameri A, Fard MRA. Application of reverse osmosis technology for arsenic removal from drinking water. Desalination. 2006;1–3:725–7.
32. Jafari A, Rezaee R, Nasseri S, Mahvi AH, Maleki A, Safari M, Shahmoradi B, Daraei H. Application of micellar enhanced ultrafiltration (MEUF) for arsenic (V) removal from aqueous solutions and process optimization. J Disper Sci Technol. 2017;38:1588–93.
33. Bahmania P, Maleki A, Daraei H, Khamforoush M, Rezaee R, Gharibi F, Tkachev AG, Burakov AE, Agarwal S, Gupta VK. High-flux ultrafiltration membrane based on electrospun polyacrylonitrile nano- fibrous scaffolds for arsenate removal from aqueous solutions. J Colloid Interf Sci. 2017;506:564–71.
34. Bahmania P, Maleki A, Rezaee R, Mahvi AH, Khamforoush M, Athar SD, Daraei H, Gharibi F, McKay G. Arsenate removal from aqueous solutions using micellar-enhanced ultrafiltration. J Environ Health Sci Engineer. 2019;17:115–27.
35. Bahmania P, Malekia A, Rezaee R, Khamforoush M, Yetilmezsoy K, Athara SD, Gharibia F. Simultaneous removal of arsenate and nitrate from aqueous solutions using micellar-enhanced ultrafiltration process. J Water Process Eng. 2019;27:24–31.
36. Bahmania P, Malekia A, Rezaee R, Khamforoush M, Yetilmezsoy K, Athara SD, Gharibia F. Application of modified electrospun nanofiber membranes with α-Fe_2O_3 nanoparticles in arsenate removal from aqueous media. Environ Sci Poll Res. 2019;26:21993–2009.
37. Kalaruban M, Loganathan P, Kandasamy J, Vigneswaran S. Submerged membrane adsorption hybrid system using four adsorbents to remove nitrate from water. Environ Sci Pollut Res Int. 2018;25(21):20328–35.
38. Singh P, Sarswat A, Pittman CU, Mlsna T, Mohan, D. Singh Sustainable Low-Concentration Arsenite [As(III)] Removal in

Single and Multicomponent Systems Using Hybrid Iron Oxide–Biochar Nanocomposite Adsorbents—A Mechanistic Study. ACS Omega. 2020.
39. Soni R, Shukla DP. Synthesis of fly ash based zeolite-reduced graphene oxide composite and its evaluation as an adsorbent for arsenic removal. Chemosphere. 2019;219:504–9.
40. Soni AB, Keshav A, Verma V, Suresh S. Removal of Glycolic Acid from aqueous solution using Bagasse Flyash. Int J Environ Res. 2012;6(1):297–308.
41. Suresh S, Srivastava VC, Mishra IM. Study of catechol and resorcinol adsorption mechanism through granular activated carbon characterization, pH and kinetic study. Sep Sci Technol. 2011;46(11):1750–66.
42. Cooper AM, Hristovski KD, Moller T, Westerhoff P, Sylvester P, Westerhoff P, Sylvester P. The effect of carbon type on arsenic and trichloroethylene removal capabilities of iron (hydr)oxide nanoparticle-impregnated granulated activated carbons. J Hazard Mater. 2010;183:381–8.
43. Kalderis D, Koutoulakis D, Paraskeva P, Diamadopoulos E, Otal E, del Valle J, Pereira CF. Adsorption of polluting substances on activated carbons prepared from rice husk and sugarcane bagasse. Chem Eng J. 2008;144:42–50.
44. Pintor AMA, Vieira BRC, Santos SCR, Boaventura RAR, Botelho CMS. Arsenate and arsenite adsorption onto iron-coated cork granulates. SciTotal Environ. 2018;642:1075–89.
45. Ocinski D, Mazur P. Highly efficient arsenic sorbent based on residual from water deironing—Sorption mechanisms and column studies. J Hazard Mater. 2020;382:1–10.
46. Muniz G, Fierro V, Celzard A, Furdin G, Gonzalez G, Ballinas MDL. Synthesis, characterization and performance in arsenic removal of iron-doped activated carbons prepared by impregnation with Fe(III) and Fe(II). J Hazard Mater. 2009;165:893–902.
47. Kleinert S, Muehe EM, Posth NR, Dippon U, Daus B, Kappler A. Biogenic Fe(III) minerals lower the efficiency of iron-mineral-based commercial filter systems for arsenic removal. Environ Sci Technol. 2011;45:7533–41.
48. Suresh S, Srivastava VC, Mishra IM. Anubhav Pratap-Singh, Multicomponent Column Optimization of ternary adsorption based removal of phenolic compounds using Modified Activated Carbon. J Environ Chem Eng. 2021;9: 104843.
49. Zhu Y, Liang M, Lu R, Zhang H, Zhu Z, You S, Liu J, Liu H. Removal of arsenic from aqueous solution by Fe(III)-impregnated sorbent prepared from sugarcane bagasse. Fresenius Environ Bull. 2011;20:1288–96.
50. Suresh S, Srivastava VC, Mishra IM. Studies of adsorption kinetics and regeneration of aniline, Phenol, 4-Chlorophenol and 4-Nitrophenol by activated carbon. Chem Ind Chem Eng Q. 2013;19(2):195–212.
51. Sigrist ME, Brusa L, Beldomenico HR, Dosso L, Tsendra OM, González MB, Pieck CL, Vera CR. Influence of the iron content on the arsenic adsorption capacity of Fe/GAC adsorbents. J Environ Chem Eng. 2014;2(2):927–34.
52. Bissen M, Frimmel FH. Arsenic — a Review. Part I: occurrence, toxicity, speciation, mobility. Acta Hydrochim Hydrobiol. 2003;31:9–18.
53. Lobo C, Castellari J, Lerner JC, Bertola N, Zaritzky N. Functional iron chitosan microspheres synthesized by ionotropic gelation for the removal of arsenic (V) from water. Inter J Biol Macromol. 2020;164:1575–83.
54. Zeng L. Arsenic adsorption from aqueous solutions on an Fe(III)-Si binary oxide adsorbent. Water Qual Res J. 2004;39:267–75.
55. Almazan-Sanchez PT, Castañeda-Juárez M, Martinez-Miranda V, Solache-Ríos MJ, Lugo-Lugo V, Linares-Hernández I. Behavior of TOC and color in the presence of iron-modified activated carbon in methyl methacrylate wastewater in batch and column systems. Water Air Soil Pollut. 2015;226:72.
56. Vitelarodriguez AV, Rangelmendez JR. Arsenic removal by modified activated carbons with iron hydro(oxide) nanoparticles. J Environ Manag. 2013;114:225–31.
57. Deliyanni E, Bandosz TJ, Matis KA. Impregnation of activated carbon by iron oxyhydroxide and its effect on arsenate removal. J Chem Technol Biotechnol. 2013;88:1058–66.
58. Nieto-Delgado C, Rangel-Mendez JR. Anchorage of iron hydro(oxide) nanoparticles onto activated carbon to remove As(V) from water. Water Res. 2012;46:2973–82.
59. Wang J, Xu W, Chen L, Huang X, Liu J. Preparation and evaluation of magnetic nanoparticles impregnated chitosan beads for arsenic removal from water. Chem Eng J. 2014;251:25–34.
60. Marques Neto JdO, Bellato CR, Milagres JL, Pessoa KD, Alvarenga ESd. Preparation and evaluation of chitosan beads immobilized with Iron(III) for the removal of As(III) and As(V) from water. J Braz Chem Soc. 2013;24:121–32.
61. Ali I, Al-Othman ZA, Alwarthan A, Asim M, Khan TA. Removal of arsenic species from water by batch and column operations on bagasse fly ash. Environ Sci Pollut Res. 2014;21:3218–29.
62. Cho DW, Jeon BH, Chon CM, Kim Y, Schwartz FW, Lee ES, Song H. A novel chitosan/clay/magnetite composite for adsorption of Cu (II) and As (V). Chem Eng J. 2012;200:654–62.
63. Elwakeel K. Removal of arsenate from aqueous media by magnetic chitosan resin immobilized with molybdate oxoanions. Int J Environ Sci Technol. 2014;11(4):1051–62.
64. Shakoor MB, Niazi NK, Bibi I, Shahid M, Saqib ZA, Nawaz MF, Shaheen SM, Wang H, Tsang DC, Bundschuh J. Exploring the arsenic removal potential of various biosorbents from water. Environ Int. 2019;123:567–79.
65. Langmuir I. The adsorption of gases on plane surfaces of glass, mica and platinum. J Am Chem Soc. 1918;40:1361–403.
66. Freundlich HMF. Over the adsorption in solution. J Phys Chem. 1906;57:385–471.
67. Temkin MI, Pyzhev V. Kinetics of ammonia synthesis on promoted iron catalyst. Acta Phys Chim USSR. 1940;12:327–56.
68. Redlich O, Peterson DL. A useful adsorption isotherm. J Phys Chem. 1959;63:1024–6.